Calibration of gain and timing mismatch for TI-ADCs with signals in all Nyquist zones using adaptive noise canceller

Dinh Thi Kim Phuong[1,2], Pham Hai Dang[3], Pham Nguyen Thanh Loan[2], Le Duc Han[3], Nguyen Duc Minh[2*]

[1]Faculty of Electronic Engineering, Hanoi University of Industry;
[2]School Electronics and Telecommunications, Hanoi University of Science and Technology;
[3]Collaboration researcher with Hanoi University of Science and Technology.
*Corresponding author: minh.nguyenduc1@hust.edu.vn.
Received 11 December 2021; Revised 26 January 2022; Accepted 14 February 2022.
DOI: https://doi.org/10.54939/1859-1043.j.mst.77.2022.137-149

ABSTRACT

This paper presents a novel all-digital background calibration technique for general Time-Interleaved Analog-to-Digital Converters (TIADCs). Calibration of gain and timing mismatch of TIADCs using the estimation technique is designed based on the principle of the Adaptive Noise Canceller (ANC). In this ANC, there are two stages in gain, timing mismatch estimation in which a cascade structure of the correction and estimation is proposed to guarantee that our calibration achieves high performance. Besides the first Nyquit zone, the input signal at different Nyquist zones is also experimented. It is shown through the result that our calibration performs excellently on all chosen Nyquist zones. It achieves the SNDR (Signal to Noise Ratio) and SFDR (Spurious Free Dynamic Range) improvement of 19dB and 49dB, respectively. Moreover, the synthesized design with hardware co-simulation carried on the Xilinx Kintex-7 field-programmable gate array (FPGA) platform consumes only 7.36 % of the hardware resources of the FPGA chip and reduces the mismatch tone level to -87 dB. In addition, our convergence speed of SNDR during calibration is approximately 1/3 others.

Keywords: All-digital feed-forward calibration; Sub-sampling TIADCs; FPGA implementation; ANC principle.

1. INTRODUCTION

Current data communication systems such as cable television transmissions, baseband optical communication, and wide-band channel require analog- to- digital converters (ADCs) with high-speed, high resolution, and energy efficiency. A time interleaved ADC (TIADC), including individual ADCs operating in parallel, both in a laboratory and even in manufacture, was incorporated into SAR-ADC (Successive Approximation Register) topology to apply to modern devices. In such a time-interleaved structure, time shifted analog- to- digital conversion of an analog signal is carried out sequentially by sub-ADCs, followed by a round-robin fashion. The first problem that need resolving is to balance the increasing conversion rate and power consumption as well as circuit area for embedded systems. In addition, TIADC performance is affected by channel mismatch consisting of offset, gain, and timing mismatch. The method in which SFDR is enhanced is currently under intense examination and may involve the decrease of gain, offset and timing mismatch by normal least mean squares (LMS) algorithm. Most of the mismatch among the individual ADC is due to some imperfection of each sub-ADC during the manufacturing process and due to voltage and temperature variation (PVT). It is necessary for all TIADCs to mitigate mismatch errors with estimation and calibration techniques.

Recently, the calibration techniques can be classified into two major categories, namely mixed-signal and all-digital calibration as in [1, 8, 13]. Mixed-signal calibration techniques mitigate the clock skew effects by employing an analog variable delay line (VDL) in each sub-ADC's clock path as in [2, 6, 7]. Meanwhile, all-digital approaches use post digital signal processing (DSP) to directly compensate for the TIADC outputs [1, 8-12, 14, 15]. Digital correction can not be

influenced by PVT (Process-Voltage-Temperature) variations and the additional jitter introduced by the VDL [16], which in turn helps to take advantage of scaled complementary metal-oxide-semiconductor (CMOS) technologies. Hence, digital calibration has recently become an outstanding technique in both the circuit design and the signal processing field.

Authors in [10, 12, 17] developed the timing mismatch calibration mechanisms for an arbitrary number of interleaved channels by using a digital synthesis filter bank in the correction phase. The mechanism consists of more than two digital adaptive filters adding to the sub-ADC outputs to mitigate the effects of timing mismatch as in [10]. More specifically, such a digital correction system requires a high complexity level as in [17], hence the power consumption and costs of large chip area slump in comparison with a digital synthesis filter bank used in multi-GS/s ADC designs as in [12].

Currently, there are two well-known estimation classes: cross-correlation based estimation [1, 8, 9, 5] and free-band based estimation[10-12, 15] to mitigate timing mismatch of TIADC. In this paper, we propose the novel estimation technique of gain and timing mismatches based on Adaptive Noise Canceller (ANC), which maximizes the output signal-to-noise ratio for any Nyquist Zone. Our approach eliminates the aforementioned mismatch band's limitations based on calibration, such as relaxing the pre-existence of an out-of-band region and removing the high-pass filter, which can reduce the complexity of hardware implementation. The digital correction is simplified by subtracting mismatch error from the TIADC output. The performance comparison between the proposed calibration and the cross-correlation based on calibration is also analyzed. The synthesized design with hardware co-simulation on XilinxKintex-7 field-programmable gate array (FPGA) platform of the proposed calibration is validated and assessed.

The structure of the rest of the paper is as follows: Section 2 analyzes the system model and presents our calibration technique based on the ANC with any Nyquist Zone. In order to show the efficiency of the proposed calibration, Section 3 analyzes simulation and experimental results with FPGA validation. Finally, conclusions are included in Section 4.

2. PROBLEM

2.1. Mismatch band based calibration reviews

A commonly known model of an M-channel TIADC with the appearance of gain and timing mismatches in sub-ADCs is shown in figure 1 as in [15]. The m^{th} channel is characterized by the gain named g_m and the timing mismatch $r_m T_s$ (r_m presents the timing mismatch relative to the overall sampling period T_s) for $m = 0,1,...,M-1$. Each input signal $x(t)$ in the different channel is multiplied by g_m at the point of $(lM+m)T_s + r_m T_s$, resulting in a sequence $y_m[l]$. The TIADC's output sequence is formed by combining the output of sub-ADCs using a multiplexer (MUX). Consequently, the sampling period of $y[n]$ is as effective as that of T_s.

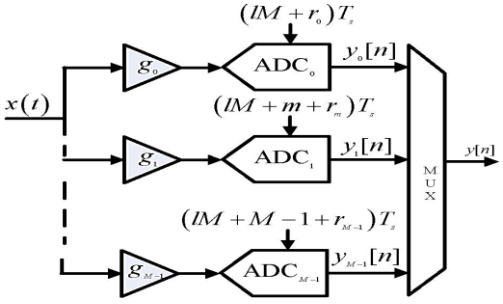

Figure 1. *An M-channel TIADC with gain and timing mismatches.*

Assuming the input signal $x(t)$ is slightly oversampled and band-limited ($X(j\Omega)=0$ for $|\Omega Ts|\geq\pi$), the discrete-time Fourier transform (DFT) of the output $y[n]$ can be expressed as in [15]:

$$Y(e^{j\omega})=\sum_{k=0}^{M-1}X\left(e^{j\left(\omega-\frac{2\pi k}{M}\right)}\right)\breve{H}_k\left(e^{j\left(\omega-\frac{2\pi k}{M}\right)}\right) \quad (1)$$

where:

$$\breve{H}_k(e^{j\omega})=\frac{1}{M}\sum_{m=0}^{M-1}g_m e^{r_m H_d(e^{j\omega})}e^{-jk\frac{2\pi}{M}m} \quad ; \quad H_d(e^{j\omega})=j\omega,\ for-\pi<\omega<\pi \quad (2)$$

and $H_d(e^{j\omega})$ is the frequency response of an ideal derivative filter [3]. $X(e^{j\omega})$ is the discrete-time spectrum of the sampled input $x[n]=x(t)|_{t=nT_s}$. If the timing skews r_m are small and by exploiting the first-order Taylor's series approximation, the frequency response of the derivative filters can be expressed as equation (3):

$$e^{jr_m H_d(e^{j\omega})}\approx 1+r_m H_d(e^{j\omega}) \quad (3)$$

Replacing (2) with (3) gives:

$$\breve{H}_k(e^{j\omega})=G_k+R_k H_d(e^{j\omega}) \quad (4)$$

where:

$$G_k=\frac{1}{M}\sum_{m=0}^{M-1}g_m e^{-jk\frac{2\pi}{M}m} \quad ; \quad R_k=\frac{1}{M}\sum_{m=0}^{M-1}g_m r_m e^{-jk\frac{2\pi}{M}m} \quad (5)$$

It is worth noting that the variables $\{G_k,R_k\}$ contain the information of the gain and timing mismatches. Obviously, $G_0=1/M\sum_{m=0}^{M-1}g_m$ is the gain mismatch average of all sub-ADCs. Generally, without loss, it can be assumed that the average value of the timing mismatches is zero, i.e., $R_0\approx 0$ or can be neglected as in [15], otherwise, the compensated signals can be $G_0x[n]$ after calibration. To be simple, we assume $G_0=1$. Under these assumptions and conditions, the inverse DFT of (1) can be written as (6):

$$y[n]=x[n]+e[n] \quad (6)$$

In (6), the error signal $e[n]$ contains all interfering terms due to gain and clock skew mismatches. In [15], the error signal is analyzed as a sum of two inner-product components for even M. It can be expressed by:

$$e[n]=c_g^T x_{g,n}+c_r^T x_{r,n} \quad (7)$$

where modulated signal vectors are defined by:

$$x_{g,n}=m_n x[n] \quad ; \quad x_{r,n}=m_n(h_d * x[n]) \quad (8)$$

$h_d[n]$ denotes the impulse response of the ideal derivative filter. The modulation vector m_n is expressed as:

$$m_n = \left(2\cos\left(1.\frac{2\pi}{M}n\right), -2\sin\left(1.\frac{2\pi}{M}n\right), ..., 2\cos\left(k.\frac{2\pi}{M}n\right), -2\sin\left(k.\frac{2\pi}{M}n\right), ..., 2\cos\left(\left(\frac{M}{2}-1\right)\frac{2\pi}{M}n\right), -2\sin\left(\left(\frac{M}{2}-1\right)\frac{2\pi}{M}n\right), (-1)^n \right) \quad (9)$$

Where T represents the matrix transpose operator. The gain and timing mismatch coefficient vectors c_g, c_r of the size $(M-1)$-by-1 are defined in terms of the real and imaginary parts of the parameters $\{G_k, R_k\}$ as in [15].

2.1.1. Digital Correction

The error signal in (7) and signal vectors in (8) are unknown since they are functions of the unknown input signals and unknown gain and clock skew parameters. Authors used the output instead of the input in blind calibration for the approximation of the error signal $e[n]$ as follows:

$$\hat{e}[n] = \hat{c}_g^T \underbrace{m_n y[n]}_{\hat{x}_{g,n}} + \hat{c}_r^T \underbrace{m_n \left(h_d[n] * y[n]\right)}_{\hat{x}_{r,n}} \quad (10)$$

$\hat{c}_g^T$ and $\hat{c}_r^T$ are estimated results of the vectors c_g^T and c_r^T, respectively. Using (6), the compensated signal can be expressed by (11) and the principle of the digital correction is performed:

$$x[n] \approx y[n] - \hat{e}[n] \quad (11)$$

2.1.2. Digital Estimation

In order to estimate the gain and timing skew coefficients $\{c_g, c_r\}$, authors in [15] assume that the input signal is a band-limited low-pass signal and that TIADC slightly oversamples the input signal. With these assumptions, oversampling results in higher frequencies containing only spurs due to the gain and timing skews, as shown in figure 2. This frequency band is called *free-band* or mismatch band. Thus, there exists an out-of-band region that contains only error spectra.

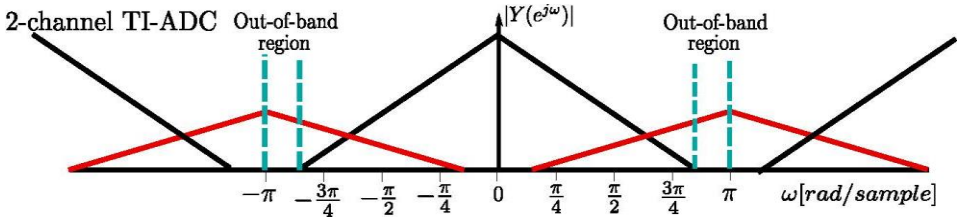

Figure 2. *The Spectrum of the TIADC output for M=2 with the present of out-of-band region (or mismatch band).*

High-Pass Filters' (HPFs) $f[n]$ are designed to filter out gain and timing mismatch inducing errors and to attenuate the input signal energy in the mismatch band. The estimated vectors $\hat{x}_{g,n}$ and $\hat{x}_{r,n}$ are also filtered through $f[n]$ to generate $\{\bar{x}_{g,n}, \bar{x}_{r,n}\}$. Note that the error $d[n]$ in *free-band* is a reference signal of the learning algorithms. The channel mismatch coefficients $\{c_g, c_r\}$ are estimated by using the LMS algorithm as in [3] to minimize the error signal $\varepsilon[n] = d[n] - \bar{e}[n]$ in the free-band region. Hence, the coefficients of c_g, c_r [15] can derive from updating equations in the adaptive LMS algorithm as in (12).

$$\hat{c}_{g,n} = \hat{c}_{g,n-1} + \mu_g \bar{x}_{g,n}^T \varepsilon[n] \quad ; \quad \hat{c}_{r,n} = \hat{c}_{r,n-1} + \mu_r \bar{x}_{r,n}^T \varepsilon[n] \tag{12}$$

Where μ_g and μ_r are the step size parameters of LMS algorithms for gain and timing mismatches, respectively. It would be worth noting that the channel mismatch coefficients are updated with an amount being cross-product of two error signals (the channel mismatch induces image signals and their estimates), hence meeting the requirements of the input statistical properties [3]. The limitations of some approaches are (i) the input signal is slightly oversampled, (ii) there exists an out-of-band region affected only by the error spectra, and (iii) the location of the mismatch band is known beforehand in order to design HPFs' $f[n]$. In other words, it puts high constraints on input spectrum because in order to get accurate estimation, the timing mismatch must be inside the mismatch band. However, it is not difficult to see that when the input signal has a limited bandwidth, all components of the error spectra fall into an out-of-band region. For example, in Fig. 3(a) and (c), some or all spurs (the small red triangles) lie completely within the original signal bandwidth (the large black triangle). The remaining smaller triangles are components of the error spectra due to mismatches.

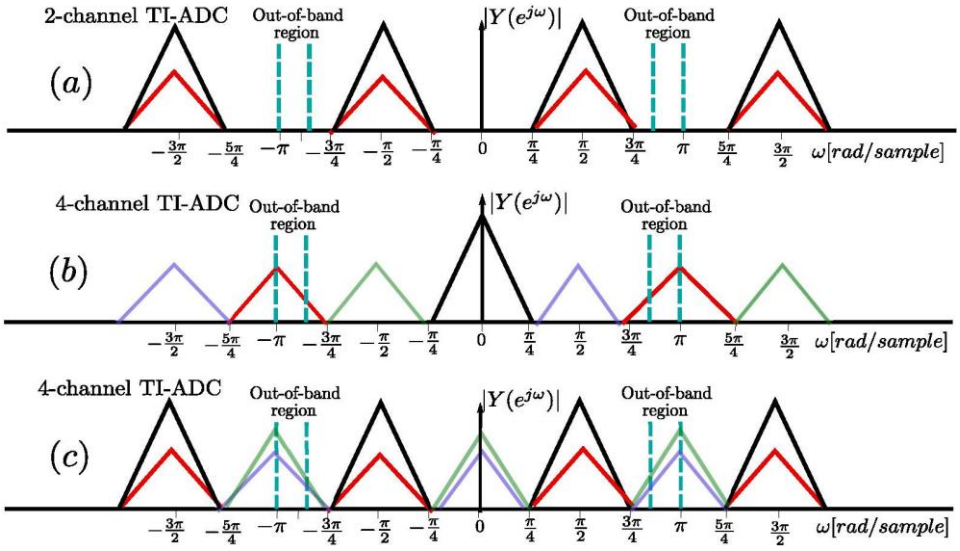

Figure 3. *The figures show the spectrum of the TIADC for* $M = 2,4$.
For (a) and (c), the lack large triangles centered at $\pm\pi/2$ *are the original spectrum; whereas, for (b), the original spectrum is centered at 0.*
The remaining smaller triangles are components of the error spectra due to mismatches.

2.2. Proposed calibration technique

2.2.1.Gain and Timing Mismatch Calibration use ANC algorithm

Free-band based adaptation is not used, thus the location of the mismatch band is no longer important in this technique. It is worth noting that the distorted output signal $y[n]$ is the sum of two components: the desired clean signal $x[n]$ and the error signal due to gain and timing mismatches. The error signal due to gain and timing mismatches is linearly presented in terms of the mismatch coefficients as expressed in (7). Using (6) and (7), we can write:

$$y[n] = \underbrace{\begin{bmatrix} x_{g,n}^T & x_{r,n}^T \end{bmatrix}}_{u_n^T} \underbrace{\begin{bmatrix} c_g \\ c_r \end{bmatrix}}_{c^0} + x[n] = u_n^T c^0 + x[n] \tag{13}$$

The error signal is the linear regression term $u_n^T c^0$ that can be constructed by a linear filter. $x[n]$ represents the signal component to be estimated. Obviously, the estimation problem is referred to as an adaptive noise canceler presented in [3] and shown in figure 4. The output of the linear filter is expressed by $\hat{e}[n] = u_n^T c_{n-1}$.

Feeding the output feedback into the linear filter and adjusting the coefficients of the linear filter via an LMS adaptive algorithm aims to minimize total system output power. Hence, this leads to an output $\hat{x}[n] = x[n] + \left(u_n^T c^0 - u_n^T c_{n-1}\right)$ that is the best fit in the least squares estimate of the signal $x[n]$ where c_{n-1} is the mismatch coefficient estimate of c_0 at $(n-1)$. Thus, the system output serves as the error signal for the adaptive process, as shown in figure 4.

Assume that the input signal $x[n]$ is a Wide-Sense Stationary (WSS), the input signal $x[n]$ is not correlated to the error signal $e[n] = u_n^T c^0$. The error signal is estimated by $\hat{e}[n] = u_n^T c_{n-1}$, and this is due to gain and timing skew mismatches. As shown in figure 4, we have (14):

$$\hat{x}[n] = y[n] - u_n^T c_{n-1} = x[n] + \left(e[n] - \hat{e}[n]\right) \tag{14}$$

Taking the square root of both sides of (14), we have (15):

$$\hat{x}^2[n] = x^2[n] + \left(e[n] - \hat{e}[n]\right)^2 + 2x[n]\left(e[n] - \hat{e}[n]\right) \tag{15}$$

Because the input signal is uncorrelated with the error signal, $E\left(e[n] - \hat{e}[n]\right) = 0$. Taking expectations of both sides, we have:

$$E\left\{\hat{x}^2[n]\right\} = E\left\{x^2[n]\right\} + E\left\{\left(e[n] - \hat{e}[n]\right)^2\right\} \tag{16}$$

Obviously, the output noise power $E\left\{\left(e[n] - \hat{e}[n]\right)^2\right\}$ is minimized when the linear filter is adjusted to minimize the output power $E\left\{\hat{x}^2[n]\right\}$. Therefore, minimizing the total output power optimizes the output signal-to-noise ratio. The coefficients can be derived by an adaptive algorithm as follows:

$$c_n = c_{n-1} - \frac{1}{2}\mu \frac{\partial \hat{x}^2[n]}{\partial c_{n-1}} \tag{17.a}$$

$$c_n = c_{n-1} + \mu u_n^T \left(y[n] - u_n^T c_{n-1}\right) \tag{17.b}$$

Where μ is the step-size. Using (14), the updating equation (17.a) can be written by (17.b).

In order to use the adaptive algorithm expressed in (17.b), the regression vector u_n is required. From (8) and (13), this regression vector undepends on the unknown signal $x[n]$. In blind calibration, we again substitute $y[n]$ for $x[n]$ in (8) to estimate the vectors $x_{g,n}, x_{r,n}$. In order to have a more accurate estimate for $x[n]$, the proposed calibration technique consists of two cascaded ANC stages, as shown in figure 5. The initial estimate $x_1[n]$ of $x[n]$ in the first ANC stage is fed into the second ANC stage in order to get a more accurate approximation of the signal vector u_n in figure 4, leading to a more precise construction of the error signal due to the gain and timing skew mismatches, i.e., $\hat{e}_1[n] \approx e[n]$.

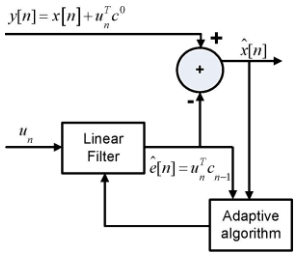

Figure 4. *Digital Estimation based on Adaptive Noise Canceller (ANC).*

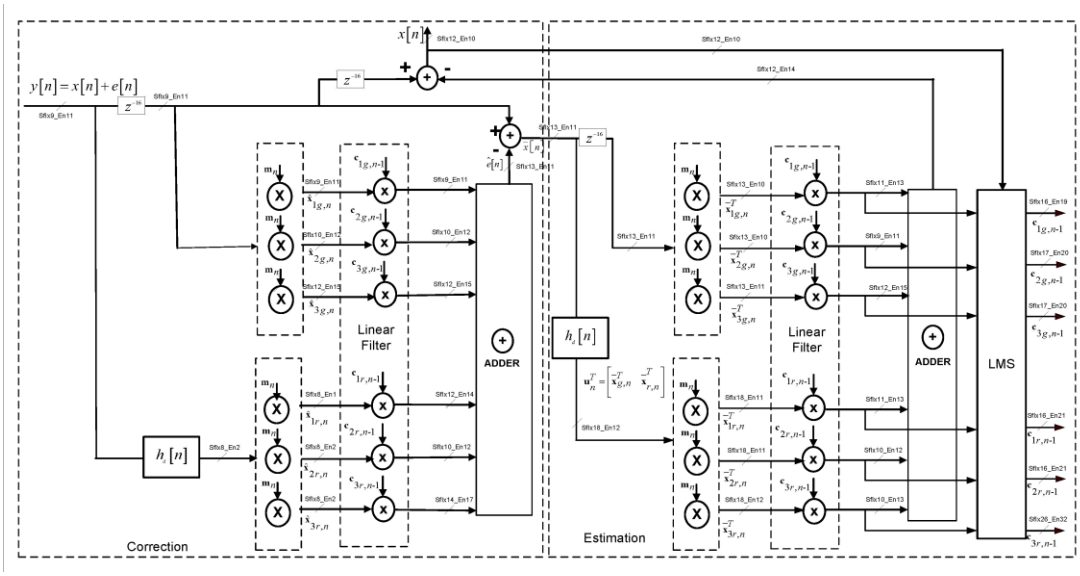

Figure 5. *Proposed digital calibration technique based on ANC.*

2.2.2.Gain and timing mismatch calibration for any Nyquist zone

The Nyquist zone (Nyquist band - NB) of the input signal is determined by k_{NB}^{th}. The bandpass (BP) is then defined by:

$$(k_{NB}-1)\frac{f_s}{2} < f_L \le |f| \le f_H < k_{NB}\frac{f_s}{2}, k_{NB} \ge 1 \ , \ k_{NB} \ge 1 \tag{18}$$

Where f_L, f_H are the lowest and highest cut off frequencies of the input, respectively.

If the condition (18) is fulfilled, there will be no aliases after sub-sampling the original input [3]. A filter is proposed to compute the derivative of the undersampling TIADC's original BP input. The filter is called a BP Derivative (BD) filter and is re-sketched in figure 6. It encompasses a scaling factor that depends on k_{NB} , and two Finite Impulse Response (FIR) filters with constant coefficients. BD filter includes a differentiator filter $h_d[n]$ and a Hilbert filter. The Hilbert filter is an all-pass filter that shifts the input signal phase by 90 degrees [3], and its impulse response $h_h[n]$ is expressed by [3]. The impulse response of the BD filter is expressed by (19):

$$h_{bd}[n] = h_d[n] + h_h[n] \times (-1)^{k_{NB}} \times \lfloor k_{NB}/2 \rfloor \times 2\pi \tag{19}$$

The constant (or scale factor) of $(-1)^{k_{NB}} \times \lfloor f_H/B \rfloor \times 2\pi$ is referred to as an input parameter of the proposed calibration algorithm and $1 \le k_{NB} \le \lfloor f_H/B \rfloor$. As shown in figure 6, the input signal

is fed both into the Hilbert filter and the derivative filter. After that, the Hilbert filter's output multiplies by the constant of $(-1)^{k_{NB}} \times \lfloor f_H / B \rfloor \times 2\pi$. Then the result is added to derivative filter's output to get x'_n . By replacing the baseband derivative filter $h_d[n]$ in figure 5 by $h_{bd}[n]$ in figure 6, our proposed solution can be applied to the input at any NZ.

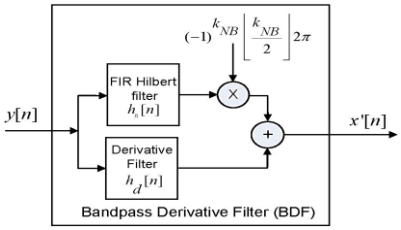

Figure 6. *Bandpass derivative filter.*

3. SIMULATION RESULTS

3.1. Input data

To verify the efficiency of the proposed technique, simulations are carried out on an undersampling four-channel TIADCs with 60 dB SNR (thermal noise level) clocked at $f_s = 2.7GHz$. Gain and timing skew mismatches are modeled as Gaussian distribution with zero mean and standard deviation δ_{ge} of 0.02, δ_{te} of 0.33ps, respectively. With $k_{NB} = \{1,2,3,4\}$ sampling rate is feasible as in [3]. Thus, the simulations demonstrate the efficiency of the proposed calibration. The number of FIR taps is designed to be equal with coefficients for both the derivative filter and Hilbert filter. The coefficients of these FIR filters are obtained by multiplying the exact coefficients by the Hanning window to mitigate the influence of a truncation error. In the simulation, the order of FIR filter chosen is 33 at which the performance saturates.

3.2. Performance system evaluation

As suggested by Proakis [3], the $1^{st}, 2^{nd}, 3^{rd}$ and 4^{th} Nyquist Zones are usually considered in sub-sampling. However, other studies have just used the 1^{st} while our proposal operates with different Nyquist bands, even with the higher ones and still achieves high the SNDR/SFDR performance. Figure 7 demonstrates the output spectrum of TIADC before and after calibration for a single-tone sinusoidal input signal at the frequency of $f_{in} = 0.45 \times f_s + f_s/2$ in the third NB. As illustrated in this figure, the spurs due to gain and timing skew mismatches are mitigated considerably in comparison with the output spectrum before calibration. The SFDR is improved by almost 41 dB, while the SNDR value after calibration is about 60 dB, which is equal to its value in the no-mismatch case.

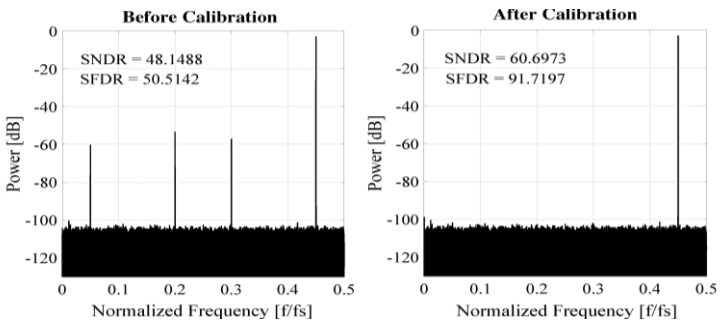

Figure 7. *The output spectrum of four channel TIADCs with input $f_{in} = 0.45 \times f_s + f_s/2$ in the third Nyquist band (Due to undersampling TIADC).*

The presented feedforward calibration is also validated for a band-limited bandpass with a multitone input signal. Figure 8 shows the output spectrum with/without calibration for a 47 sinusoidal tone input in the second NB with $f_L = 0.05\times f_s + f_s/2$, and $f_H = 0.4\times f_s + f_s/2$. As illustrated in Figure 8, the bandpass input is down-converted directly to frequency baseband $(0, f_s/2)$ by undersampling TIADC where f_H and f_L map are $0.1 f_s$ and $0.45 f_s$ due to the second NZ sub-sampling, respectively. It can be seen that spurs due to gain and timing skews are reduced to the noise floor. The proposed calibration is also applied to a 16 quadrature amplitude modulation (16-QAM) input signal with 10MHz bandwidth at the carrier frequency $0.45\times f_s + f_s/2$. In order to make pulse shaping, a relatively FIR square root raised cosine filter with a roll-off factor of 0.3 is used. As a result, shown in figure 9, all spurious errors due to gain and timing skew are mostly suppressed, and again, the distortion is significantly reduced to the noise floor.

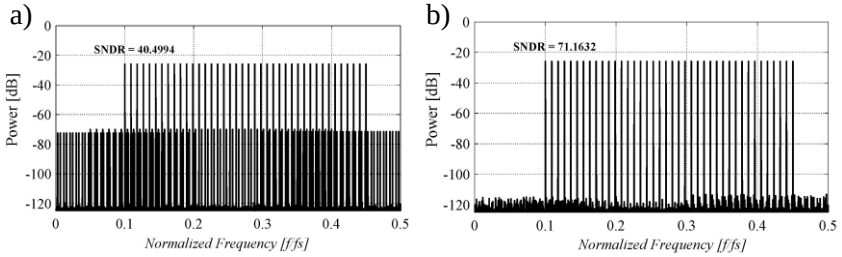

Figure 8. *The output spectra for the band-limited bandpass multitone input in the second Nyquist zone (a) without, and (b) with calibration.*

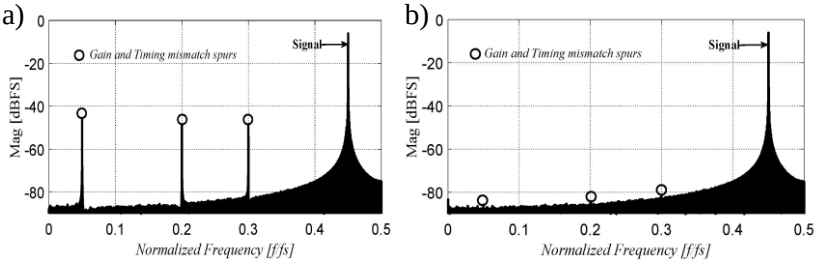

Figure 9. *The output spectra for the 16-QAM signal with a carrier frequency of* $0.45\times f_s + f_s/2$ *and 10MHz bandwidth (a) without, and (b) with calibration.*

Figure 10 a, 10 b shows the performance of SNDR and SFDR of gain and timing mismatch calibration using ANC technique combined with a bandpass derivative filter for signals of the first four Nyquist zones. The result is: with gain and timing mismatch, before calibration, the higher the order of the Nyquist bands is, the lower the SNDR and SFDR are reduced.

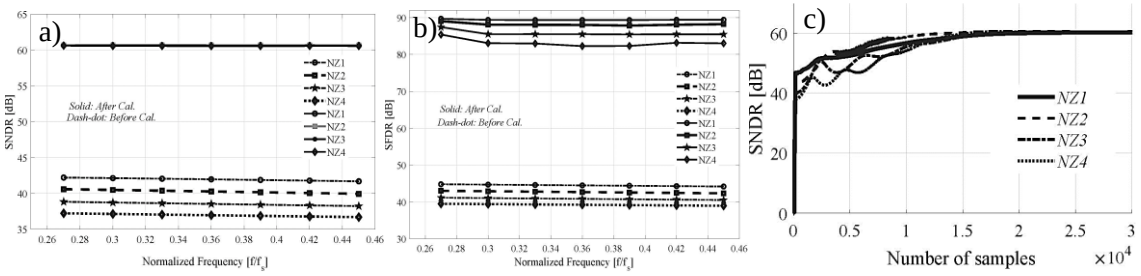

Figure 10. *Performance of SNDR/SFDR of TIADC for single tone inputs of the first four NB with and without calibration. (a) Performance of SNDR of TIADC. (b) Performance of SFDR of TIADC; (c) Convergence speed behavior during calibration with the first four NB.*

However, the effect of correcting these mismatches based on ANC algorithm still guarantees the improvement of approximately 19 dB of SNDR and approximately 49 dB of SFDR. As can be concluded from figure 10, before calibration, the rise of input frequency leads to the growth of timing skew, which has a large impact on TIADC. In addition, the derivative filter employs to decouple timing skew mismatch, the estimated signals in (3) are computed using sub-ADC outputs in place of an input. Therefore, the estimated signal becomes less accurate when input frequency increases. On account of these, after calibration, the SNDR value after calibration is approximately 60 dB which means there is no mismatch while the SFDR value is enhanced by about 41 dB with different Nyquist zones. Besides, as can be seen from figure 10.c, the convergence speed in different Nyquist zones is nearly the same, at about 18K samples.

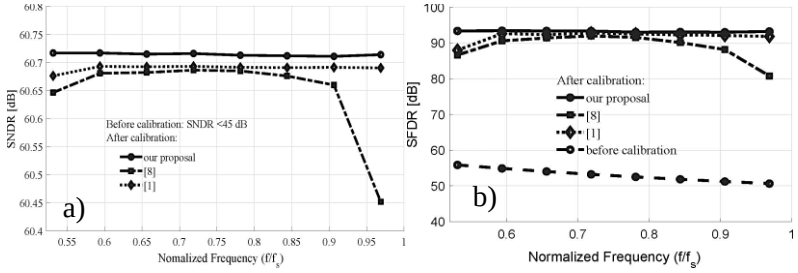

Figure 11. *Comparison SNDR/SFDR vs. input frequencies at the second Nyquist zone between our proposal technical and other technical.*

Table 1. *Simulated SNDR and SFDR performance comparison input signal in the 3rd , 4th NB.*

Frequency (MHz)		**The 3rd NB**				**The 4th NB**			
		2835	**3555**	**3690**	**3915**	**4185**	**4905**	**5040**	**5265**
SNDR without cal.(dB)		41.572	41.488	41.397	41.264	41.472	41.276	41.191	41.073
SNDR with cal. (dB)	[1]	60.590	60.577	60.492	60.203	60.610	60.605	60.602	60.601
	[8]	60.387	60.685	60.683	57.165	59.495	60.485	60.483	58.165
	Our approach	**60.687**	**60.664**	**60.658**	**60.663**	**60.678**	**60.663**	**60.661**	**60.660**
SFDR without cal.(dB)		49.852	48.742	48.030	47.486	49.852	48.742	47.030	46.486
SFDR with cal. (dB)	[1]	88.71	88.594	88.403	88.464	86.71	87.094	86.903	86.403
	[8]	79.851	85.894	85.130	75.727	76.851	85.894	85.130	71.727
	Our approach	**91.696**	**92.394**	**92.464**	**91.903**	**89.696**	**89.394**	**89.464**	**89.015**

Figure 11 shows the SNDR/SFDR performance over the second, the third and the fourth Nyquist band, respectively, compared with previous studies [1, 8]. In SFDR as well as SNDR graph, two-dash curve with square makers represents the result shown in [1], dotted curve with rhombus makers represents the result shown in [8], and solid curve with circle makers represents the signal in our proposal after calibration and long-dash curve with circle markers illustrates SFDR performance before calibration. Based on these graphs, it is pointed out that SNDR and SFDR value in our technique is slightly higher than those of the aforementioned, especially when the frequency is approximately $k f_s/2$ the calibration value in our technique remains stable while there was a sharp reduction in the result of [8]. Also, in [1, 8], only clock skews mismatch are calibrated, while both gain and timing skew mismatches are calibrated in our technique. That is the reason why figure 11 uses the δ_{ge} of $0, \delta_{te}$ of 0.33ps for our simulation. The same conclusions are witnessed in the 3rd and 4th Nyquist zone, which are demonstrated in the following table 1.

Figure 12 illustrates the comparison of convergence speed of gain and timing mismatch estimates

in our proposed technique with that in the mentioned studies. It can be seen that it took them about 50K samples to get the expected value, while it only takes us 18K samples to do the same.

With these above results, it is obvious that our techniques could be used on all Nyquist zones without harming the efficiency.

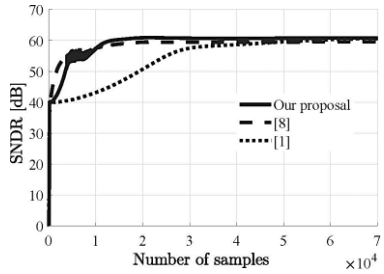

Figure 12. *Time evolution of SNDR during calibration.*

3.3. Hardware Implementation and Validation

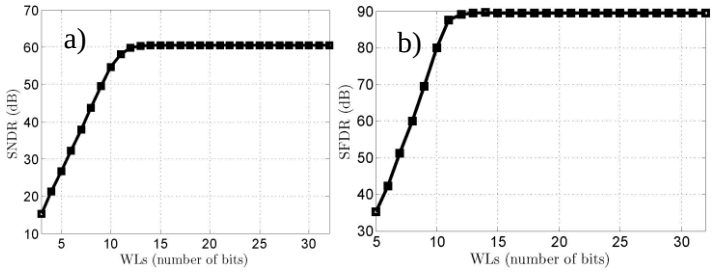

Figure 13. *SNDR/SFDR vs. WLs of the compensated TIADC output: (a) SNDR; (b) SFDR.*

Table 2. *FPGA Synthesis Results.*

Family	**Xilinx Kintex-7**
Device	XC7K325T
Logic cells utilization	6,777/203,800 (3.33%)
Distributed LUT RAM	177/64,000 (0.28%)
Flip-Flop (FFs)	6,053/407,600 (1.49%)
DSP slices	19/840 (2.26%)
Fmax	204.25 MHz

A field-programmable gate array (FPGA) design flow using Matlab/Simulink in [13] is applied in our framework. In order to implement the all-digital calibration algorithm on FPGA, the hardware architecture of the proposed calibration is designed and optimized in terms of fixed-point representation of signals. The signal Word-Length (WL) is defined by signal ranges, which is the span of numbers that a fixed-point data type and the scale are used to convert signal values into a binary representation. The signal WLs influence on SNDR and SFDR performance metrics of the calibration system. In the optimal fixed-point (OFxp) hardware model, as figure 5, its parameters such as the order of FIR filters and the signal WLs need to be optimized. Figure 5 shows the optimal fixed-point (OFxp) hardware architecture of the proposed calibration, processing real-time signal data in a sample-by-sample manner. The z^{-k} blocks are delayed/pipeline registers. The notation of *sfix9En11* presents a 9-bit signed fixed-point data type with a Fraction-Length (FL) or fractional bits of 11. The delays are made suitable. The pipeline registers are inserted to reduce the combinational path length and improve the overall working frequency and throughput. The latency between the distorted output and the compensated output is 32 clock cycles. Figure 13 presents SNDR and SFDR performance with the number of bits (or WL) assigned to the compensated TIADC output. As can be seen, the optimal values of WL of

the compensated TIADC output is 11 bits in order to get the best trade-off between the performance and hardware cost. The synthesized circuit is proved to operate properly on the FPGA and to consume very little hardware resources of the FPGA chip, as reported in table 2.

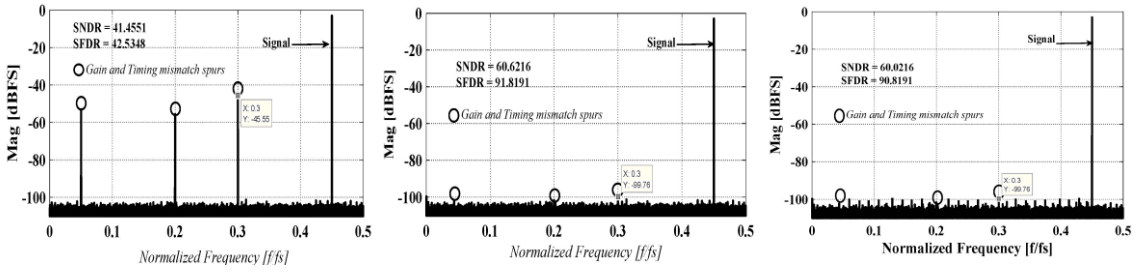

Figure 14. *PSD of the compensated TIADC output with floating-point and fixed-point data: (a) PSD of signal before calibration; (b)PSD of signal after calibration with floating-point model; (c)PSD of signal after calibration with fixed-point model.*

As illustrated by figure 14, at the 3th Nyquist zone, before calibration, the spur value is about -37dB, while the calibration was illustrating result without converting floating-point to fixed-point shows that the spurs value is at about – 87 dB, nearly the same with the practical result with the convert of floating-point to the fixed point. The output spectrum with/without calibration for single tone input in the third NB with $f = 0.45 \times f_s + 3 f_s/2$. As illustrated in figure 15, the signal input is down-converted directly to frequency baseband by undersampling TIADC where input frequency maps is $0.45 f_s$ due to the third NZ sub-sampling. It can be seen that spurs due to gain and timing skews are reduced to the noise floor.

4. CONCLUSION

This paper presents the all-digital background calibration technique of the gain and timing mismatches in TIADC for input at any NBs. The gain and timing mismatch coefficients are estimated based on adaptive noise canceller. The simulation results show the efficiency of the proposed calibration, obtaining SNDR improvement of around 19 dB, SFDR improvement of approximately 49 dB with the 4-channel TIADC, which is sampled at 2.7 GHz on any Nyquist zone. The optimal hardware architecture of the proposed technique is developed and correctly validated on the Xilinx Kintex-7 board, which houses the Kintex-7 FPGA chip XC7K325T. The synthesized result shows that the digital circuit operates properly on the FPGA and utilizes a small number of hardware resources of the FPGA chip (only 7.36% of the hardware resources of the FPGA chip and reduces the mismatch tone level to -87 dB). The proposed hardware architecture converges after 18K samples (or 6.67 μs). In addition, our convergence speed of SNDR during calibration is faster than others. This means that this technique is also feasible with ASIC implementation, even with higher Nyquist zones.

Acknowledgment: *This research is funded by Hanoi University of Industry and EDABK Laboratory, Hanoi University of Science and Technology.*

REFERENCES

[1] . H. L. Duc et al.*,"Fully digital feed forward background calibration of clock skews for sub-sampling tiadcs using the polyphase decomposition,"* IEEE Transactions on Circuits and Systems I: Regular Papers, **Vol. 64**, No. 6 (2017), pp. 1515–1528.

[2] . B. Razavi, *"Design Considerations for Interleaved ADCs,"* IEEE Journal of Solid-State Circuits, **Vol. 48**, No. 8 (2013), pp. 1806–1817.

[3] . J. G. Proakis and D. G. Manolakis, *"Digital Signal Processing: Principles, Algorithms and Applications,"* Upper Saddle River, New Jersey (2007).

[4] . P. Diniz, *"Adaptive Filtering: Algorithms and Practical Implementation,"* Kluwer international series

in engineering and computer science, Springer (2008).
[5] . H. Le Duc et al., *"A Fully Digital Background Calibration of Timing Skew in Undersampling TI-ADC,"* IEEE 12th International in New Circuits and Systems Conference (NEWCAS) (2014).
[6] . D. Camarero et al., *"Mixed-Signal Clock-Skew Calibration Technique for Time-Interleaved ADCs,"* IEEE Transactions on Circuits and Systems I: Regular Papers, **Vol. 55**, No. 11 (2008), pp. 3676–3687.
[7] . A. Haftbaradaran and K. W. Martin, *"A sample-time error compensation technique for time-interleaved adc systems,"* IEEE in Custom Integrated Circuits Conference (CICC) (2007), pp. 341–344.
[8] . H. Le Duc et al., *"All-Digital Calibration of Timing Skews for TIADCs Using the Polyphase Decomposition,"* IEEE Transactions on Circuitsand Systems II: Express Briefs, **Vol. 63** (2016).
[9] . J. Matsuno et al., *"All-Digital Background Calibration Technique for Time-Interleaved ADC Using Pseudo Aliasing Signal,"* IEEE Transactions on Circuits andSystems I: Regular Papers, **Vol. 60**, No. 5 (2013), pp.1113–1121.
[10] .P. Satarzadeh et al., *"A parametric polyphase domain approach to blind calibration of timing mismatches for M-channel time-interleaved ADCs,"* Proceedings of 2010 IEEE International Symposium on Circuits and Systems (ISCAS), (2010), pp. 4053–4056.
[11] .V. Divi and G. W. Wornell, *"Blind Calibration of Timing Skew in Time-Interleaved Analog-to-Digital Converters,"* IEEE Journal of Selected Topics in Signal Processing, **Vol. 3**, No. 3 (2009), pp. 509–522.
[12] . S. Huang and B. Levy, *"Blind Calibration of Timing Offsets for Four-Channel Time-Interleaved ADCs,"* IEEE Transactions on Circuits and Systems I: Regular Papers, **Vol. 54**, No. 4 (2007), pp. 863–876.
[13] .Le Duc Han, Thi Kim Phuong Dinh, Van-Phuc Hoang, and Duc Minh Nguyen. *"All-digital background calibration of gain and timing mismatches in time-interleaved ADCs using adaptive noise canceller,"* AEU-International Journal of Electronics and Communications 114 (2020): 152999.
[14] . J. A. McNeill et al., *"Split ADC' Calibration for All-Digital Correction of Time-Interleaved ADC Errors,"* IEEE Transactions on Circuits and Systems II: Express Briefs, **Vol. 56**, No. 5 (2009), pp. 344–348,.
[15] .C. Vogel et al., *"Adaptive blind compensation of gain and timing mismatches in M-channel time-interleaved ADCs,"* 15th IEEE International Conference on Electronics, Circuits and Systems ICECS (2008), pp. 49–52.
[16] .S. Chenet al., *"All-digital calibration of timing mismatch error in time-interleaved analog-to-digital converters,"* IEEE Transactions on Very Large Scale Integration (VLSI) Systems, **Vol. 25,** No. 9 (2017), pp. 2552–2560.
[17] .P. P. Vaidyanathan, *"Multirate Systems and Filter Banks,"* Upper Saddle River, NJ, USA:Prentice-Hall, Inc.(1993).

TÓM TẮT

Hiệu chỉnh mất tương thích độ khuếch đại và mất tương thích thời gian của bộ chuyển đổi tương tự số đan xen thời gian (TIADC) với các tín hiệu ở các miền Nyquist sử dụng nguyên tắc lọc nhiễu thích nghi

Bài báo trình bày một kỹ thuật hiệu chỉnh hoàn toàn ở miền tín hiệu số cho bộ chuyển đổi tương tự số, lấy mẫu xen kẽ theo thời gian của các sub-ADC (TIADC). Việc hiệu chỉnh mất tương thích độ khuếch đại và mất tương thích thời gian của TIADC bằng kỹ thuật ước lượng được thiết kế dựa trên nguyên tắc bộ lọc thích nghi loại bỏ nhiễu (ANC). Trong nguyên tắc ANC này, có hai tầng để ước lượng mất tương thích thời gian và độ khuếch đại giữa các sub- ADC, trong đó cấu trúc phân tầng của hiệu chỉnh và ước lượng được đề xuất đảm bảo đạt được hiệu suất cao. Ngoài các tín hiệu vào ở vùng Nyquit đầu tiên, các tín hiệu vào tại các vùng Nyquist khác nhau cũng được thử nghiệm. Kết quả là kỹ thuật hiệu chỉnh của chúng tôi thực hiện được trên tất cả các vùng Nyquist khác nhau. Kết quả đã cải thiện được mức của SNDR và SFDR lần lượt là 19 dB và 49 dB. Hơn nữa, tổng hợp thiết kế với mô phỏng phần cứng được thực hiện trên nền tảng FPGA Xilinx Kintex-7 chỉ tiêu thụ 7,36% tài nguyên phần cứng của chip FPGA và giảm biên độ của các hài mất tương thích xuống mức -87 dB. Đồng thời, thời gian hội tụ của việc ước lượng chỉ bằng 1/3 thời gian của một số tác giả khác.

Từ khoá: Hiệu chỉnh có phản hồi miền tín hiệu số, Lấy mẫu phụ TIADCs, Thực thi FPGA, Nguyên tắc lọc thích nghi loại bỏ nhiễu.